Mohamed Zaidan QAWAQZEH

Al-Balqa Applied University, Jordan

doi:10.15199/48.2020.04.13

Design and computation of a suspended magnetic separator for processing metallurgic slag

Abstract. *A new design of metallurgic slag processing electromagnetic separator on basis of a cylindrical extracting electromagnet has been presented and method of its design based on computation of 3-D field distribution by means of space integral equation method using Radia® modulus has been offered.*

Streszczenie. *W artykule zaprezentowany został nowy projekt obróbki żużla metalurgicznego za pomocą elektromagnesu cylindrycznego. W realizacji projektu przedstawiono symulację komputerową na bazie obliczeń pola elektromagnetycznego 3D metodą całkową przy wykorzystaniu pakietu oprogramowania Radia® . (**Projekt i obliczenie zawieszonego separatora magnetycznego w obróbce żużla metalurgicznego**).*

Keywords: metallurgic slag, magnetic separator, computer simulation.
Słowa kluczowe: żużel metalurgiczny, separator, symulacja komputerowa

Introduction

The amount of industrial metallurgic slag rises as production of ferrous metals increases. Metal lost with slag not only decreases the output noticeably, but also complicates significantly further slag processing. Therefore, improvement of metallurgic slag processing workflows with maximal metal extraction is one of the ways making it possible to increase metal smelting without involving additional material and raw resources into metallurgic cycle. Slag mineral component used to produce crushed rock and granular slag, when slag melt is processed with water, is also an important raw material resource. Both components are widely used in construction, and presence of metal worsens their quality greatly.

As it can be seen from practice, the major reasons for low level of metal utilization from slag are insufficient research and absence of specialized magneto-separating equipment, adapted to conditions of slag processing. Application of outfit designed for mineral dressing or protection of production equipment to process metallurgic slag is ineffective because of significant scrap slagging (the amount of the extracted metal does not exceed 30−40 % of its content in the slag) [1].

Out of all the variety of separators (using pulleys, drums, suspension, etc.) produced nowadays the most relevant, according to many criteria, design of a separator built in existing slag processing manufacturing flowsheet, as well as newly developed, is a suspended separator design. This design is the most universal from the point of view of location in any place of a transporting conveyer; it does not have strict overall dimension limitations, which provides the opportunity to create a longer zone along the belt with the aim of effective extraction of ferromagnetic objects. Removal of ferromagnetic bodies out of the flow of the material without gripping its non-ferrous fraction is an additional merit of a suspended separator. Analysis of these separators designs proves that work on creation and improvement of separating devices in the world is directed at:

- increased efficiency of extraction due to magnetic field intensification and time of its action on material being separated;
- increased reliability of unloading extracted bodies when minimal non-magnetic material is gripped;
- decreased material and power consumption.

It can be achieved by both improvement of methods of traditional device designing and development of new separator electromagnetic systems.

The purpose of the paper

The aim of the paper is development of a new design of a suspended electromagnetic separator, providing a more effective extraction of metal out of slag, and working out the method of its designing based on 3-D field distribution.

Design of a suspended separator for processing metallurgic slag

Taking into account result of the analysis of known designs, with the aim of solving this problem, the authors offered a design of a suspended separator, based on a cylindrical extracting electromagnet (CEEM), meeting the processing conditions of most metallurgic and steel-casting slag (Fig.1).

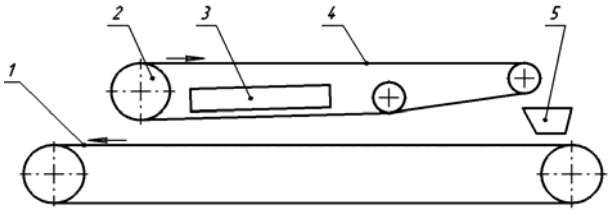

Fig. 1. Suspended separator for extracting metal from slag: 1 − feeding belt conveyer; 2 – unloading electromagnetic pulley; 3 – extracting cylindrical electromagnet with non-magnetic insert; 4 – unloading belt; 5 – reservoir for extracted metal

The main special features of the design are:

- top unloading of the separator;
- use of a typical cylindrical extracting electromagnet as a separator extracting electromagnet;
- use of a non-magnetic insert in the outer ring pole of the extracting electromagnet.

Application of top unloading of the separator provides the use of a more efficient principle of its assembly, i.e. along the belt of the main feeding conveyer.

To make clear the interaction of the separator structural parts, let us consider the separation process.

When conveyer belt 1 moves in the direction of the arrow the separated slag goes into the working area of the separator. Here, under the action of magnetic field created by CEEM 3, ferromagnetic inserts contained in the slag mass are extracted and pressed to the surface of the unloading belt 4. Then during the motion together with the unloading belt 4 the extracted ferromagnetic inserts go to the zone of action of electromagnetic pulley 2, with the help of which they are held during the passage onto the upper part of the unloading belt 4, where they are unloaded into a reservoir for metal 5.

In spite of the fact that the scheme “extracting electromagnet – transporting electromagnet”, used in the design, showed itself well, the unloading efficiency was low because of unstable passing of the extracted metal from a more powerful extracting electromagnet 3 to a less powerful unloading pulley 2.

To improve the conditions of such a passing it was offered to provide the outer ring pole 1 of CEEM with a non-magnetic insert 5 on the side facing the pulley (Fig. 2).

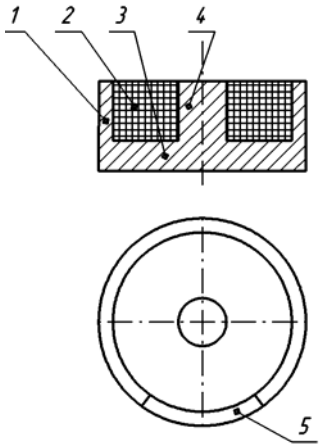

Fig. 2. CEEM with a non-magnetic insert: 1 – outer ring pole; 2 − magnetizing coil; 3 – yoke; 4 – core; 5 – non-magnetic insert

Such a design of the ring pole also helps to decrease the effect of shunting the unloading electromagnetic pulley magnetic field by the field of extracting electromagnet [2].

Computation mathematical model of an extracting magnet

A priori a separator extracting electromagnet should provide a large depth and reliability of extraction along the whole length of the feeding conveyer. To ensure this condition, taking into consideration technological features of application and wide dimensional range of slag separators, the design method should consider a number of parameters, such as separator suspension height, granulometric composition and density of separated slag, range of ferromagnetic inserts dimensions etc. However, cylindrical electromagnetic systems with open boundary working field have been insufficiently investigated and there is practically no information necessary for their computation and designing, and similar systems with opening have not been investigated at all.

That is why it is an urgent problem to develop a method of computation of rational parameters of a cylindrical electromagnetic system with open boundary working field, making it possible to obtain the main geometric parameters of magnetic circuit and magnetizing winding, and the values of its electrical parameters with minimal resource and time consumption.

The method of space integral equations was used during mathematical modeling (Fig. 3) as the main computation method, as it does not require any additional boundary conditions and is based only on the general integral expression of field intensity through magnetization of magnetic system parts [3–4].

$$\vec{H} = \frac{1}{4\pi}\left[\int_V \frac{\left(\nabla\vec{M}\right)\vec{r}_{QM}}{r_{QM}^3}dV - \int_S \frac{\left(\vec{n}\vec{M}\right)\vec{r}_{QM}}{r_{QM}^3}dS\right] + \frac{1}{4\pi}\int_{V_P} \frac{\vec{J}\vec{r}_{QP}}{r_{QM}^3}dV_P \quad (1)$$

where $\vec{H}$ is magnetic field strength in the observation point Q; $\vec{r}_{QM}$ is a radius vector connecting observation point Q with the current integration point M concerning magnetic circuit steel; $\vec{r}_{QM}$ is a radius vector connecting observation point Q with the current point P of integration concerning magnetization coil; V, S are volume and surface of all the ferromagnetic elements of the magnetic system, correspondingly; V_p is volume of the magnetization coil; $\vec{J}$ is vector of magnetization coil current; $\vec{n}$ is an outer normal to surface S in integration point (Fig. 3).

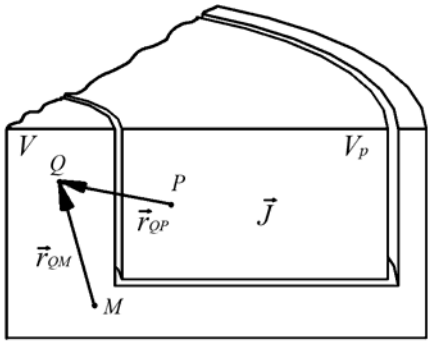

Fig.3. Magnetic system mathematical model

The solution of this integral equation can be obtained by means of approximate numerical methods. With this purpose the area of integration is divided into a finite number of elements and integral is changed to its approximate value as a final sum. In this way, an integral equation is reduced to a system of non-linear algebraic equations. Solving the obtained system one should determine distribution of elements magnetization, after that compute the magnetic field strength in the required points. In this way, magnetic system mathematical model is reduced to a discrete model.

Modulus Radia® (European Synchronotron Radiation Facility) [5], integrated into Mathematica® system was applied to create a magnetic system 3-D model of extracting magnet, being chosen from a variety of systems realizing space integral equations method.

The working order concerning modulus Radia® is similar to working orders of most systems realizing methods of final and boundary elements and consists of the following stages: building models of structural elements of the core and magnetization coil, representation of model area properties, computation and obtaining computation results [5].

Development of discrete mathematical model of the magnetic circuit in modulus Radia® consists in the correct dividing it into separate geometric parts and creating a mathematical description for each of them. Modulus Radia® functions of “Field Sources” group are used to build mathematical description of the magnetic circuit geometry.

Magnetic properties of the magnetic circuit material were assigned as a non-linear dependence [6] corresponding to magnetization curve of steel, from which the magnetic circuit was made (functions group of “Magnetic Materials” of modulus Radia®).

When mathematical description of all the magnetic circuit geometric parts was made they were joined into one computation container (Fig. 4).

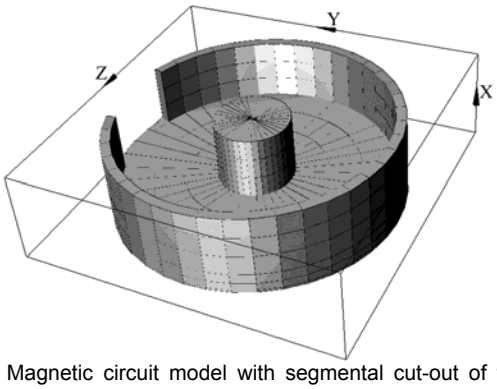

Fig. 4. Magnetic circuit model with segmental cut-out of the ring pole

Magnetization coil model is built in a similar way, by assigning its geometric dimensions using a special function from "Field Sources" group. Magnetic permeability of the coil material and current concentration (corresponding to given coil magnetomotive force $F = 9000$ A) were assigned as magnetizing coil properties.

Complete 3-D presentation of built discrete mathematical model of CEEM with open boundary working area is shown in Fig. 5.

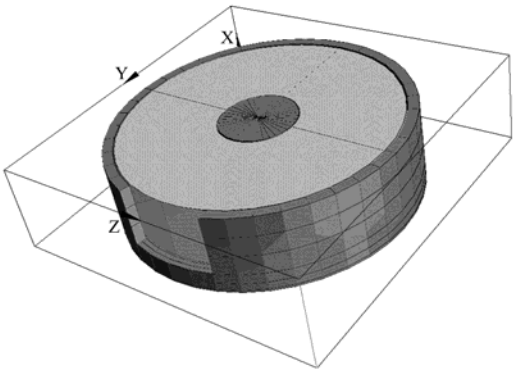

Fig. 5. Discrete mathematical model of a cylindrical extracting electromagnet

Computation of the built discrete mathematical model of magnetic system in modulus Radia® is not difficult and is carried out with the help of "Field computation" functions. Parameters, limiting the computation time (maximal number is N iterations), and determining the accuracy σ of the computation, are the parameters of the functions of this group. The following values of the parameters were taken for the computation: iterations number $N = 1000$, computation accuracy $\sigma = 0.000001$.

The computation of integral indices was made over characteristic points situated on the axis of symmetry of the magnetic system, which are shown in Fig. 6 at the distance $L = (5 - 90)$ mm from the surface of the magnetic system with discreteness of 5 mm.

Points 3 and 3* are situated on a circle with the diameter $d_3 = D_c + d_0$, points 4 and 4* are situated on a circle with the diameter $d_4 = D_p + H_p$.

The results of the considered discrete model field B_C induction computation with the help of modulus Radia® are given in the table 1. It can be seen from presented results, as it was supposed, a cut-out in the outer ring pole noticeably reduces magnetic field induction in the area of passing extracted fraction from cylindrical electromagnet to the unloading pulley (point 4).

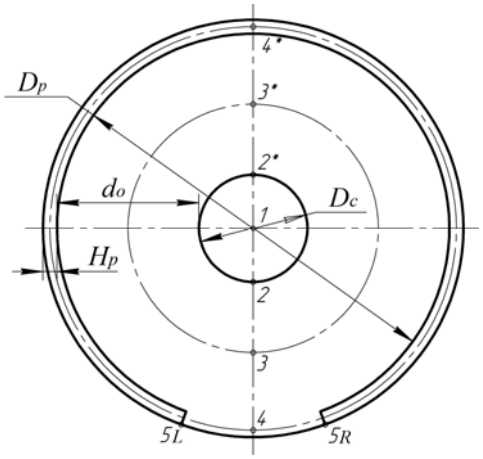

Fig. 6. The location of the characteristic points (D_c is core diameter, H_p is pole thickness, D_p is pole inner diameter, d_0 is distance between the core and the pole)

Experimental research

The research was conducted on a physical model of an electromagnetic washer. For experimental research, a physical model of an electromagnetic washer was developed and made on a linear scale of 1:5. The magnetic circuit parts of the model were made of soft magnetic annealed steel, similar in magnetic properties to cast steel, used in the industrial manufacture of iron separator magnetic circuits. The surfaces of the mutual abutment of the core, yoke, and the ring pole were made with a high degree of accuracy and surface cleanliness to ensure minimum gaps between the elements of the magnetic circuit.

The magnetizing coil of the physical model was made without a frame and was isolated with a herringbone tape impregnated with varnish and subsequent baking. To ensure the necessary magnetizing forces in all modes of the magnetic load of the iron separator the coil was solid till it filled the inter-polar window.

The coil of the physical model was powered from a rheostatic rectifier with magnetizing current control by ammeter of 0.2 accuracy class.

The magnetic field induction in the working area was measured (0.5 accuracy class) with a probe of a cross section of 4x0.8 mm. The measurements were carried out above the characteristic points of the central section shown in Fig. 6.

The magnetic field strength corresponding to each obtained value of the magnetic induction was determined by formula

$$H = \frac{B}{\mu_0}, \tag{2}$$

where μ_0 – magnetic permeability of the air ($\mu_0 = 4\pi \cdot 10^{-7}$ Hn/m).

Table 1 contains the results of measurement of magnetic B_E induction above the characteristic points shown in Fig. 6. Table 2 contains corresponding values of the magnetic field H_E strength calculated by (2) (wherein y – the distance from the surface of the poles).

Fig. 7 shows the magnetic field strength dependences on distance y above the characteristic points in CEEM working zone. Fig. 8 contains the graphs of distribution of the magnetic field strength in CEEM working zone at different distances from CEEM poles surface.

Table 1. Magnetic system working area magnetic induction computed with Radia®

№ point	1		2		2*		3		3*		4		4*		5L		5R	
L [mm]	Induction B_E / B_C [mT]	Δ [%]	Induction B_E / B_C [mT]	Δ [%]	Induction B_E / B_C [mT]	Δ [%]	Induction B_E / B_C [mT]	Δ [%]	Induction B_E / B_C [mT]	Δ [%]	Induction B_E / B_C [mT]	Δ [%]	Induction B_E / B_C [mT]	Δ [%]	Induction B_E / B_C [mT]	Δ [%]	Induction B_E / B_C [mT]	Δ [%]
5	197/199.6	-1.3	300/298.4	0.5	305/308.5	-1.1	77/81.7	-5.8	85/90	-5.6	27/28.9	-6.6	57/62.5	-8.8	66/62.2	6.1	68/62.2	9.3
10	182/185.3	-1.8	200/203.4	-1.7	218/205	6.3	73/77.7	-6	80/82.2	-2.7	25/27	-7.4	43/45.8	-6.1	38/38.8	-2.1	39/38.8	0.5
15	171/172.6	-0.9	170/165.3	2.8	178/166.5	6.9	67/71	-5.6	75/74.8	0.3	24/25.2	-4.8	34/37	-8.1	28/30.1	-7	28/30.1	-7
20	152/153.6	-1	140/138.2	1.3	147/139.2	5.6	61/64.6	-5.6	69/67.8	1.8	22/23.6	-6.8	28/30.5	-8.2	23/25.2	-8.7	24/25.2	-4.8
25	134/134.2	-0.1	118/117.4	0.5	120/118.2	1.5	56/58.7	-4.6	62/61.2	1.3	21/22.1	-5	25/26.2	-4.6	20/22.1	-9.5	21/22.1	-5
30	117/116.4	0.5	100/100.8	-0.8	102/101.5	0.5	50/53.1	-5.8	56/55.1	1.6	20/20.6	-2.9	22/23.2	-5.2	19/19.9	-4.5	20/19.9	0.5
35	101/100.8	0.2	88/87.3	0.8	88/87.8	0.2	45/48.1	-6.4	50/49.5	1	19/19.3	-1.6	19/20.8	-8.7	17/18.2	-6.6	18/18.2	-1.1
40	87/87.4	-0.5	75/76	-1.3	76/76.4	-0.5	41/43.4	-5.5	45/44.5	1.1	17/18	-5.6	18/18.9	-4.8	16/16.7	-4.2	16/16.7	-4.2
45	75/75.9	-1.2	65/66.5	-2.3	66/66.7	-1	36/39.2	-8.2	40/40	0	16/16.8	-4.8	16/17.3	-7.5	15/15.5	-3.2	14/15.5	-9.7
50	66/66.3	-0.5	57/58.4	-2.4	57/58.6	-2.7	33/35.5	-7	35/36	-2.8	15/15.7	-4.5	15/15.9	-5.7	13/14.4	-9.7	13/14.4	-9.7
55	55/58	-5.2	48/51.5	-6.8	51/51.6	-1.2	30/32.1	-6.5	32/32.4	-1.2	14/14.7	-4.8	14/14.7	-4.8	13/13.5	-3.7	12.5/13.5	-7.4
60	50/51	-2	43/45.5	-5.5	45/45.6	-1.3	27/29.1	-7.2	28/29.3	-4.4	12.5/13.7	-8.8	13/13.6	-4.4	12/12.6	-4.8	12/12.6	-4.8
65	44/44.9	-2	38/40.4	-5.9	39/40.5	-3.7	24/26.4	-9.1	25/26.5	-5.7	12/12.8	-6.3	12/12.7	-5.5	12/11.8	1.7	11/11.8	-6.8
70	38/39.8	-4.5	33/35.9	-8.1	35/36	-2.8	22/23.9	-7.9	23/24	-4.2	11/12	-8.3	11/11.8	-6.8	11/11.1	-0.9	11/11.1	-0.9
75	34/35.3	-3.7	30/32.1	-6.5	30/32.1	-6.5	20/21.8	-8.3	20/21.8	-8.3	11/11.2	-1.8	10/11	-9.1	10/10.4	-3.8	10/10.4	-3.8
80	30/31.4	-4.5	27/28.7	-5.9	28/28.7	-2.4	18/19.8	-9.1	18/19.8	-9.1	10/10.5	-4.8	10/10.3	-2.9	10/9.7	3.1	10/9.7	3.1
85	27/28.1	-3.9	24/25.8	-7	24/25.7	-6.6	17/18.1	-6.1	17/18	-5.6	9/9.8	-8.2	9/9.6	-6.3	9/9.1	-1.1	9/9.1	-1.1
90	24/25.1	-4.4	21/23.2	-9.5	22/23.2	-5.2	15/16.5	-9.1	15/16.4	-8.5	9/9.2	-2.2	8.5/9	-5.6	9/8.6	4.7	9/8.6	4.7

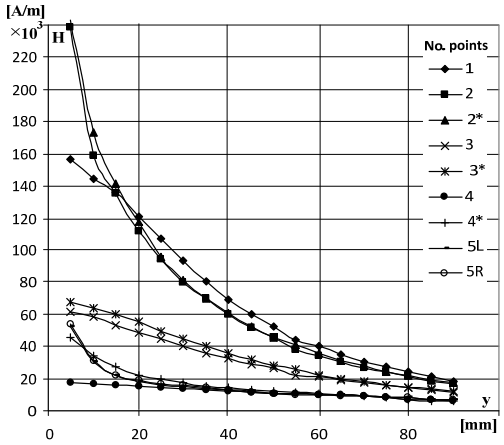

Fig. 7. The dependences of the magnetic field strength in CEEM working zone above the characteristic points

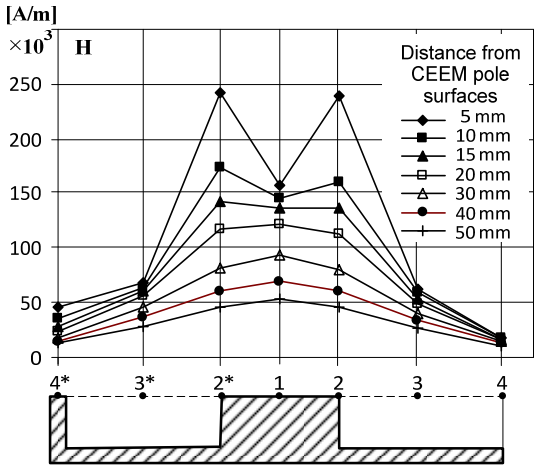

Fig. 8 The distribution of the magnetic field strength in CEEM working zone above the characteristic points

The calculation of the extractive force

The electromagnetic force parameter $HgradH$ was calculated to assess how the cut in the external ring pole influences CEEM extractive ability. The parameter is determined by the design of the electric magnet and is the criterion of the force created by it. $HgradH$ was calculated in the direction in which the extractive force is created, i.e. perpendicularly to the electromagnet poles surface.

$$HgradH \approx H\frac{\partial H}{\partial y}. \tag{3}$$

To calculate $HgradH$ the numerical differentiation formulae were used [7]. According to [7], the numerical differentiation results are greatly affected by the experiment noise: even small errors in the experimental data strongly distort the results of numerical differentiation. Therefore, it is necessary first to smooth out the experimental data, and then apply certain methods of numerical differentiation.

The results were smoothed according to the linear smoothing formulae at five points [7]:

$$\left.\begin{aligned}
\tilde{y}_0 &= \frac{1}{5}(y_{-2}+y_{-1}+y_0+y_1+y_2),\\
\tilde{y}_{-1} &= \frac{1}{10}(4y_{-2}+3y_{-1}+2y_0+y_1),\\
\tilde{y}_1 &= \frac{1}{10}(y_{-1}+2y_0+3y_1+4y_2),\\
\tilde{y}_{-2} &= \frac{1}{5}(3y_{-2}+2y_{-1}+y_0-y_2),\\
\tilde{y}_2 &= \frac{1}{5}(-y_{-2}+y_0+2y_1+3y_2),
\end{aligned}\right\} \tag{4}$$

where $\tilde{y}_0$ – the smoothed value of the function at point 0, $\tilde{y}_{-1}, \tilde{y}_1, \tilde{y}_{-2}, \tilde{y}_2$ – respectively the values of the function at the last (point -1, point 1) and the last but one (point -2, point 2) smoothed points at both ends of the values range; y_0 – the value of the function at the smoothing point 0, y_{-1}, y_1, y_{-2}, y_2 – the values of the function at the points adjacent to the point with the value of function y_0 on both sides along which the results are smoothed.

The smoothed data were differentiated in two adjacent points according to formulae [7]:

$$y_0' = \frac{1}{h}\left(\frac{y_1 - y_{-1}}{2}\right); \tag{5}$$

the formulae for the initial and the final points were used, respectively:

$$y_0' = \frac{1}{2h}(-3y_0 + 4y_1 - y_2), \tag{6}$$

$$y_0' = \frac{1}{2h}(3y_0 - 4y_{-1} + y_{-2}), \tag{7}$$

where $y_0^{'}$ – a derivative function at the point with the value of function y_0, y_0 – the value of the functions at the point at which differentiation is performed, y_{-1}, y_1, y_{-2}, y_2 – the values of the function at the points adjacent to the value of function y_0, on both sides along which differentiation was performed, h – differentiation step. In this case, the step of differentiation is taken equal to the interval of the distance of measuring the inductance in the working space.

Table 3 contains the electromagnetic force parameter values calculated according to (3) and using numerical differentiation formulae (5 – 7). Fig. 9 contains the graphs of the distribution of the parameter of the electromagnetic force in the working zone of the electromagnetic washer. The graphs are created according to the data of Table 3. Fig. 9, a contains graphs for all the characteristic points, Fig. 9, b contains graphs for points 3, 4, 3*, 4*, 5L, 5R. Fig. 10 shows the distribution of the electromagnetic force parameter $HgradH$ in CEEM working zone for different values of the distance from CEEM pole surface.

Table 2. The values of the magnetic field strength in CEEM working zone

y [mm]	Magnetic field strength H, ×10^3 [A/m]								
	1	2	2*	3	3*	4	4*	5L	5R
5	156.8	238.7	242.7	61.27	67.64	17.51	45.36	52.52	54.11
10	144.8	159.2	173.5	58.09	63.66	16.71	34.22	30.24	31.04
15	136.1	135.3	141.7	53.32	59.68	15.92	27.06	22.28	22.28
20	121	111.4	117	48.54	54.91	15.12	22.28	18.3	19.1
25	106.6	93.9	95.49	44.56	49.34	14.32	19.89	15.92	16.71
30	93.11	79.58	81.17	39.79	44.56	13.53	17.51	15.12	15.92
35	80.37	70.03	70.03	35.81	39.79	12.73	15.12	13.53	14.32
40	69.23	59.68	60.48	32.63	35.81	11.94	14.32	12.73	12.73
45	59.68	51.73	52.52	28.65	31.83	11.14	12.73	11.94	11.14
50	52.52	45.36	45.36	26.26	27.85	10.35	11.94	10.35	10.35
55	43.77	38.2	40.58	22.28	25.46	10.35	11.14	10.35	9.55
60	39.79	34.22	35.81	21.49	22.28	9.95	10.35	9.55	9.55
65	35.01	30.24	31.04	19.1	19.89	9.55	9.55	9.55	8.75
70	30.24	26.26	27.85	17.51	18.3	8.75	8.75	8.75	8.75
75	27.06	23.87	23.87	15.92	15.92	7.96	7.96	7.96	7.96
80	23.87	21.49	22.28	14.32	14.32	7.16	7.16	7.96	7.96
85	21.49	18.3	19.1	12.73	13.53	7.16	6.37	7.6	7.16
90	18.3	16.71	17.51	11.14	11.94	6.37	6.37	7.16	7.16

Table 3. The values of the parameter of the electromagnetic force in CEEM working zone

y [mm]	HgradH, ×10^9 [A^2/m^3]								
	1	2	2*	3	3*	4	4*	5L	5R
5	391.7	1452	1573.6	53.17	61.92	2.82	53.26	76.34	79.9
10	361.2	1224.3	1327.7	49.35	57.67	2.66	45.35	61.94	64.75
15	334.62	968.4	1038.5	45.66	54.03	2.53	35.3	44.56	46.73
20	308.26	575.24	645.28	42.8	51.11	2.42	22.71	22.04	23.07
25	282.11	322.94	373.11	38.14	47.43	2.28	12.98	8.94	9.28
30	241.08	224.38	247.02	32.66	42.14	2.15	7.95	4.81	5.53
35	188.79	153.6	164.89	27.73	35.88	2.02	5.57	3.31	4.06
40	146.86	110.18	112.37	23.36	29.21	1.71	4.1	2.64	3.27
45	109.88	81.83	80.47	18.56	23.53	1.34	2.9	2.06	2.59
50	79.29	59.82	59.77	14.63	19.17	1.11	2.31	1.57	1.87
55	58.75	43.87	44.43	11.62	15	0.99	1.95	1.31	1.25
60	44.22	32.73	33.35	9.17	11.58	0.94	1.65	1.09	0.9
65	31.93	23.35	25.34	7.05	9.41	1.04	1.53	0.89	0.71
70	23.83	17.77	19.72	5.9	7.22	1.03	1.39	0.83	0.68
75	19.27	14.15	15.02	5.33	5.47	0.97	1.14	0.79	0.64
80	15.19	11.03	11.61	4.57	4.59	0.9	0.93	0.69	0.56
85	12.52	9.32	9.97	4.05	4.01	0.77	0.85	0.59	0.59
90	10.82	8.1	8.7	3.54	3.56	0.69	0.78	0.56	0.56

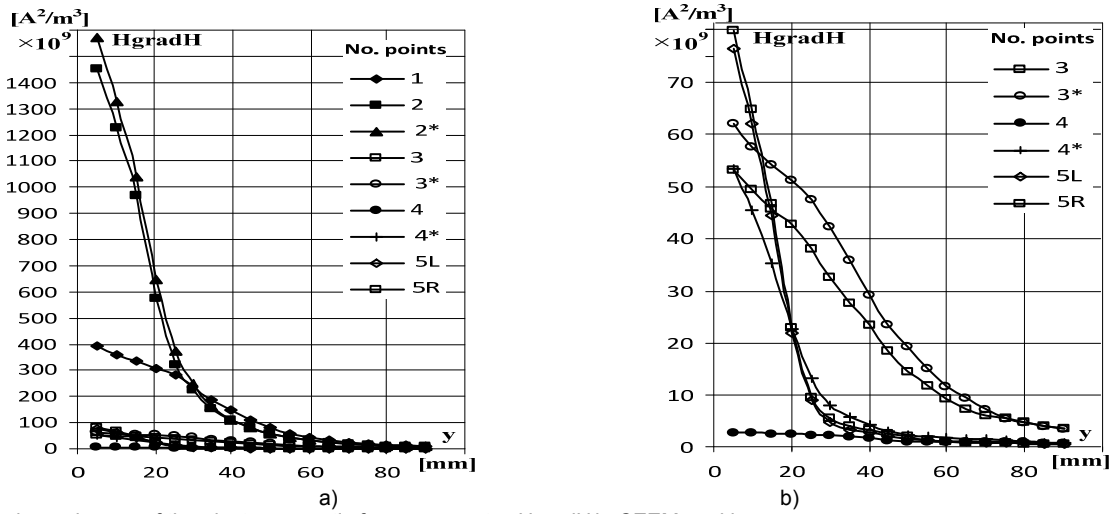

Fig. 9. The dependences of the electromagnetic force parameter *HgradH* in CEEM working zone

The graphs demonstrate that in CEEM unloading zone (point 4) for the distance values up to 500 mm from the surface of the electromagnetic washer the magnetic field strength H and the magnetic force parameter $HgradH$ essentially decrease as compared with point 4*, which provides the improvement of the unloading conditions in this range of distances. The graphs also demonstrate that at points 5L and 5R the magnetic field strength and the electromagnetic force parameter are even higher than at point 4* (especially at close distances). Research should be carried out in this direction. There are two possible solutions: a change in the configuration of the edge of the poles (rounding) or an increase in the nonmagnetic gap.

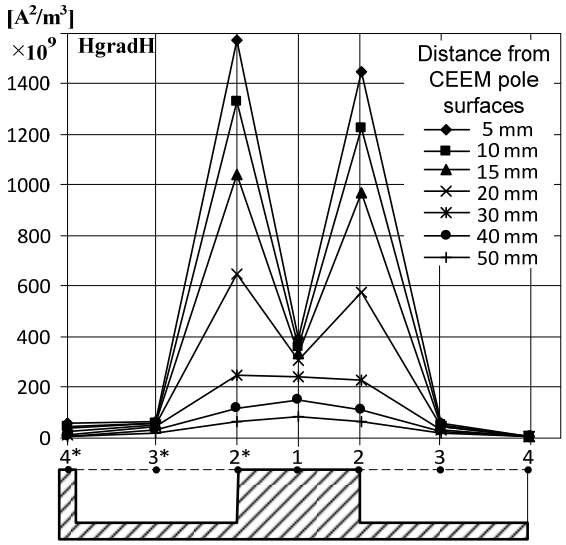

Fig. 10. The distribution of the electromagnetic force parameter *HgradH* above the characteristic points in CEEM working zone

Thus, if we assume that the magnetic force is applied to the center of the extracted body, then the minimum distance from CEEM surface, on which the extracted material will be transferred from CEEM to the electromagnetic pulley, will be 10 mm, and the maximum – 21 mm (when recalculated to the scale of the model). As can be seen from the obtained calculation, the extracting magnetic force in the unloading zone (point 4) for a smaller body will decrease by 17 times, for a larger one – by 9.4 times compared with point 4*.

Conclusion

1. The presence of a cut in CEEM external ring pole significantly reduces the magnetic field strength and the magnetic force parameter in the unloading zone, which improves the conditions for unloading the extracted material.

This iron separator is designed to operate as a part of a metallurgical slag processing line and is intended for the extraction of scrap with a particle size of 40 to 150 mm. When recalculated to the scale of the experimental CEEM model, the range of sizes of the extracted material is from 8 to 30 mm. When the distance at which the extracted material will be transferred is determined, the thickness of the conveyor belt and the technological gap between the surface of the electromagnet and the conveyor belt should also be taken into account. Their sum will be 30 mm and when recalculated to the scale of the model – 6 mm.

2. The developed suspended electromagnetic separator, when used in metallurgic slag processing complexes, will make it possible to improve the level of separation of metal inserts from mineral component, which, in its turn, will increase the quality of construction materials made from this component and will raise the output of useful metal.

3. Proposed method is acceptable for carrying out of computations of 3-D considered magnetic systems and its application results in significant reduction of the necessary resources and time for designing desired magnetic systems and to carry out their optimization in a comparatively simple way.

***Author**: PhD, Associate professor, Mohamed Zaidan Qawaqzeh, Al-Balqa' Applied University, Ma'an University College, Maan, Jordan, P.O. Box 194, 19117, E-mail: qawaqzeh@bau.edu.jo.*

REFERENCES

[1] Bryizgunov K.A., Gavrilova O.N., Donbass metallurgic slag. Donetsk: Donbass, 1989. 80 p. (in Russian)
[2] Zagirnyak M.V., Vlasov V.M., Kuznetsov M.I., Podorozhniy S.V., Suspended electromagnetic iron separator device, Ukraine Patent 6337, June 11, 2004. (in Ukrainian)
[3] Binns K.J., Lawrenson P.J., Trowbridge C.W., The Analytical and Numerical Solution of Electric and Magnetic Fields, John Wiley & Sons Publishers, 1992, 486 p.
[4] Akimov O.S. Development of mathematical model and computation of electromagnetic drum-type separator by boundary element method. *Computer Engineering in Applied Electromagnetizm*. Edited by S. Wiak, A. Krawczyk and M. Trlep. Springer, 2005. 237–242.
[5] Radia documentation Reference Guides and samples. http://www.esrf.eu/Accelerators/Groups/InsertionDevices /Software/Radia/Documentation
[6] Zagirnyak M.V., Branspiz Yu.A, Shvedchikova I.A, Magnetic separators. Design problems. Monograph. K.: Technica, 2011, 223 p. (in Russian)
[7] Rumshynskii L.Z., Mathematical processing of measurement results. M.: Nauka, 1971. (in Russian)